Angio-Stitch: An Unsupervised Coarse-to-Fine Framework for Sequential Stitching of Confocal Laser Endomicroscopy Images

Xiaoshi Hu[1], Huahui Zhang[1], Xiang Deng[1], Xiaoyue Liu[1], Peng Wang[2], and Xuesong Ye[1(✉)]

[1] Biosensor National Special Laboratory, College of Biomedical Engineering and Instrument Science, Zhejiang University, China
[2] Hangzhou Xianao Technology Inc, China

Abstract. Microvascular remodeling is a critical hallmark of early-stage tumorigenesis. While Confocal Laser Endomicroscopy (CLE) enables *in vivo* "optical biopsy" of the microvasculature, its restricted field of view (FoV) limits the assessment of macroscopic pathological continuity. To bridge this gap, we propose Angio-Stitch, an unsupervised deep learning framework tailored for multi-image stitching of hepatic microvascular sequences. Unlike existing deep learning methods primarily optimized for dual-image natural scenes—which are prone to cumulative errors in long sequences—our model adopts a robust coarse-to-fine alignment strategy. Specifically, we utilize a ResNet-based encoder integrated with a Vascular-aware Perception Transformer (VPT) to extract robust semantic features amidst speckle noise. A mesh-based deformation network is then employed to correct non-rigid tissue distortions. To explicitly preserve microvascular topology, we introduce a novel Vascular Structure Loss ($\mathcal{L}_{vsl}$) based on multi-scale Hessian responses. We evaluate our approach on the CLE-LMV dataset, established via a custom-developed NIR-CLE system. Experimental results demonstrate that Angio-Stitch achieves state-of-the-art performance in geometric accuracy and structural fidelity. This approach effectively provides clinicians with a wide-field, seamless visualization for reliable diagnostic support. Code available at: https://github.com/xiaoshihu8/Angio-Stitch

Keywords: Confocal Laser Endomicroscopy · Image Stitching · Hepatic Microvasculature.

1 Introduction

Microvascular alterations, such as neo-angiogenesis and capillary remodeling, are fundamental hallmarks of early-stage hepatic pathologies. While wide-field endoscopic modalities lack the spatial resolution to visualize 1–2 µm capillary networks, Confocal Laser Endomicroscopy (CLE) provides a powerful "optical biopsy" alternative [9][28]. It enables real-time, *in vivo* cellular-level visualization of liver micro-anatomical structures without traditional physical tissue excisions.

Despite its high resolution, CLE's clinical application is hindered by an extremely restricted Field of View (FoV, typically < 500 µm). In highly vascularized organs like the liver, this "keyhole vision" deprives clinicians of essential macroscopic context, leading to fragmented diagnostic information and an increased risk of missing subtle micro-lesions[26]. Therefore, FoV expansion is a pressing clinical necessity to bridge the gap between microscopic detail and macroscopic context, ultimately providing diagnostic support.

To mitigate this limitation, image stitching is commonly used to fuse consecutive frames into panoramas. Traditional methods rely on handcrafted features (e.g. SIFT) and geometric transformations for image alignment[17] [7] [30] [16] [12]. However, liver CLE images typically feature low contrast, repetitive textures, and a lack of salient edges. Furthermore, the probe's sliding motion causes complex non-rigid tissue deformations. Consequently, traditional techniques often suffer from feature matching failures, misalignment, and severe ghosting artifacts, failing to meet high-fidelity medical imaging standards.

In recent years, unsupervised deep learning for image stitching has demonstrated remarkable efficacy in resolving complex geometric challenges. UDIS2 [22] initially established a robust baseline by mitigating large parallax artifacts via elastic warping. Building upon this foundation, StabStitch2 [23] further refined spatial alignment by introducing bidirectional spatial warps to minimize structural distortions. Subsequently, RopStitch [24] developed an optimal plane-based framework to suppress irregular deformations and preserve structural fidelity. Extending these spatial modeling capabilities, SV-UDIS [15] addressed the extreme viewpoint disparities inherent in surround-view multi-camera systems.

However, applying current state-of-the-art methods to CLE liver images yields suboptimal results[29]. Primarily optimized for natural scenes and dual-image stitching, these models struggle to align the fine-grained, low-contrast, and repetitive textures of microscopic biological tissues[25]. Furthermore, during the continuous multi-image stitching of highly deformable soft tissues, existing spatial transformations suffer from severe error accumulation[8]. This leads to global structural distortions and the potential loss of critical pathological details.

To address these critical challenges, we proposes Angio-Stitch, a deep multi-image stitching network tailored specifically for CLE liver image sequences. Angio-Stitch overcomes the limitations of traditional image stitching by using feature interaction and deformation constraints to accurately model non-rigid deformations in microscopic tissues. Even without strong textural cues, the proposed framework achieves precise alignment across sequential images and reduces error accumulation, providing clinicians with wide-field, seamless, high-fidelity panoramic views of liver tissue.

The main contributions of this paper are as follows: 1) We establish Angio-Stitch, a deep multi-image stitching framework for CLE hepatic microvasculature, achieving field-of-view expansion for clinical diagnostic support. 2) We construct a Vascular-aware Perception Transformer (VPT) and introduce a Vascular Structure Loss ($\mathcal{L}_{vsl}$), systematically overcoming speckle noise and preserving non-rigid microvascular topologies. 3) The method achieves state-of-the-art

stitching performance on CLE-LMV (a real CLE dataset), featuring minimal ghosting and superior objective metrics.

2 Methodology

The proposed Angio-Stitch framework is illustrated in Fig. 1, mainly includes three stages: **Feature extraction and mask constraint**, **coarse-to-fine two-stage registration**, and **multi-image stitching**.

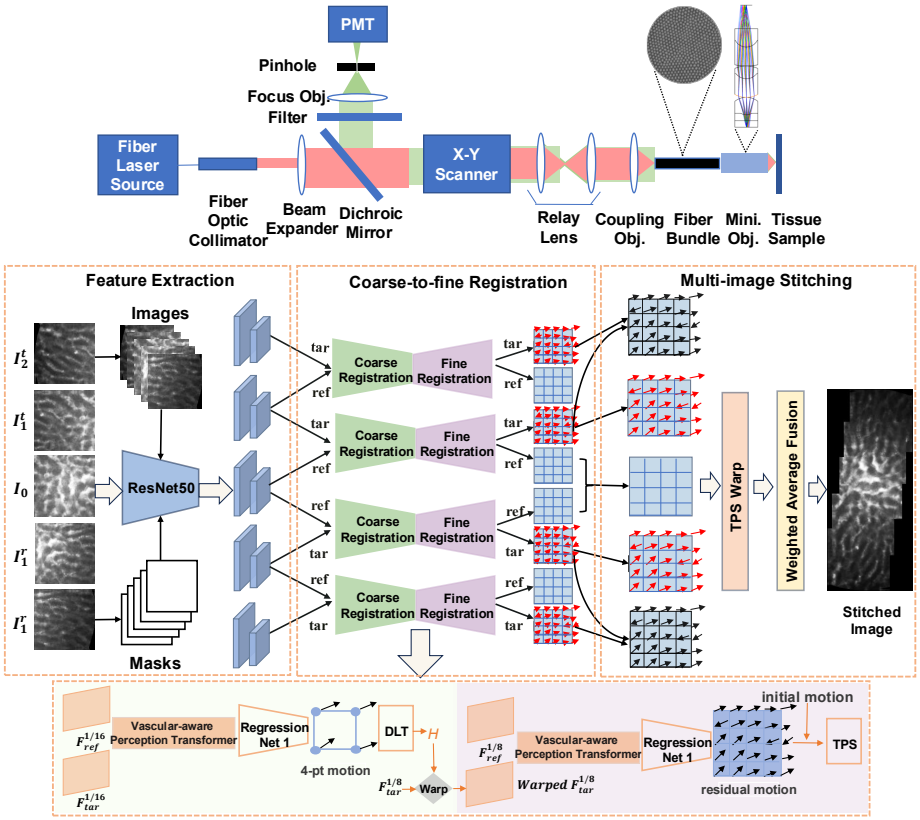

Fig. 1. The framework of Angio-Stitch.

In the first stage, a pre-trained ResNet-50 [10] extracts dual-scale feature maps: $F^{1/8}$ for fine details and $F^{1/16}$ for global semantics. To explicitly suppress invalid dark backgrounds, dynamically rescaled binary masks are element-wise multiplied with both maps, yielding the masked $F^{1/8}$ and $F^{1/16}$.

In the second stage, we propose the Vascular-aware Perception Transformer (VPT) on adjacent image pairs to sequentially regress global homography[6] and

local mesh displacements, achieving coarse-to-fine registration. Detailed elaboration in Sec.2.1.

In the third stage, the multi-image sequence is synthesized onto an adaptively sized unified canvas. Adjacent homography matrices are chain-propagated[15] to a central anchor. Each image then undergoes TPS transformation[2], followed by an intensity-weighted average fusion to seamlessly preserve the structural continuity of the hepatic microvasculature.

2.1 Coarse-to-fine Two-stage Registration

Vascular-aware Perception Transformer (VPT) To address matching challenges in CLE images caused by speckle noise and homogeneous textures, we propose the Vascular-aware Perception Transformer (VPT), as shown in Fig. 2. Replacing the standard CCL[21], the VPT maps arbitrary features into a 128-dimensional space via a dynamic adapter, outputting a sub-pixel accurate, 2-channel feature flow field $\in \mathbb{R}^{B\times 2\times H\times W}$ to drive displacement regression.

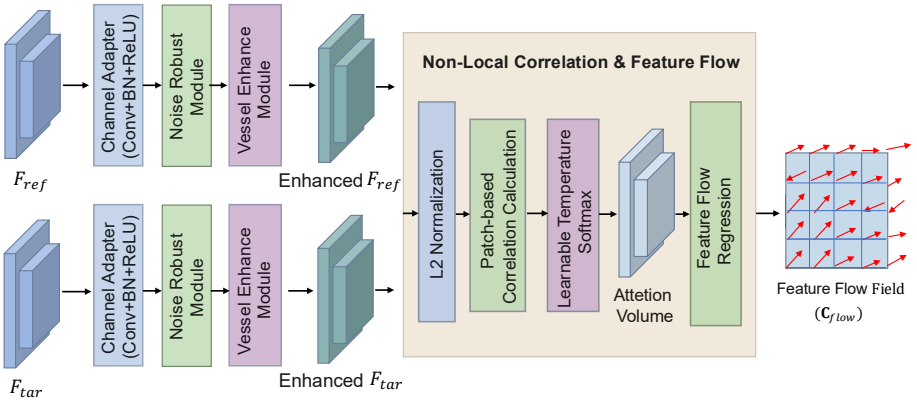

Fig. 2. Vascular-aware Perception Transformer (VPT) Module.

To handle CLE-specific artifacts, the VPT integrates a **Noise Robust Module** and a **Vessel Enhance Module**. The former employs cascaded 3×3 convolutions and a learnable residual parameter (γ) to filter speckle noise while preserving structural integrity. The latter utilizes a dual-attention mechanism combining channel attention with a large-field (7×7) spatial branch to selectively amplify the morphology of tubular hepatic sinusoids [27]. Finally, the VPT computes dense non-local correlations using 3×3 patch-based matching with a learnable temperature-scaled Softmax. By calculating the mathematical expectation of displacements over dynamic coordinate grids, the module yields a differentiable, structure-sensitive feature flow that accurately captures complex non-rigid vascular correspondences across varying clinical resolutions[3].

Coarse Registration (VPT-based Global Homography Estimation) At the coarse scale, we designate the image closer to the sequence center as the reference I_r and the peripheral image as the target I_t. The VPT module extracts a vascular-aware correlation volume from the $F_{\text{ref}}^{1/16}$ and $F_{\text{tar}}^{1/16}$ feature maps. A shallow regression network subsequently predicts the 4-pt homography parameterization[14], representing the corner displacement vectors of I_t. This motion is converted into a 3×3 matrix H via the normalized Direct Linear Transform (DLT) algorithm [1] to achieve initial global geometric alignment.

Fine Registration (VPT-based Sparse Mesh TPS Deformation) At the fine scale, $F_{\text{tar}}^{1/8}$ is geometrically pre-warped using the estimated matrix H to yield coarsely aligned features $\hat{F}_{\text{tar}}^{1/8}$. The VPT module then computes high-resolution local correlations between $F_{\text{ref}}^{1/8}$ and $\hat{F}_{\text{tar}}^{1/8}$. Following this, a deeper regression network predicts the residual motion for an evenly divided grid of $(U+1) \times (V+1)$ control points. By superimposing this residual motion onto the initial regular mesh, the network generates a non-rigid deformation field[5]. Finally, TPS transformation is applied to perform fine-grained deformation, explicitly modeling the complex non-rigid variations of hepatic microvasculature for clinical diagnostic support.

2.2 Loss Function

The framework is optimized end-to-end via a joint objective:

$$\mathcal{L}_{total} = \lambda_1 \mathcal{L}_{align} + \lambda_2 \mathcal{L}_{dist} + \lambda_3 \mathcal{L}_{rect} + \lambda_4 \mathcal{L}_{vsl} \tag{1}$$

where $\mathcal{L}_{align}$, $\mathcal{L}_{dist}$, and $\mathcal{L}_{rect}$ are consistent with [15].

To explicitly preserve hepatic microvasculature topologies for reliable clinical diagnosis, we propose a novel Vascular Structure Loss ($\mathcal{L}_{vsl}$):

$$\mathcal{L}_{vsl} = \mathcal{L}_{ssim} + \gamma_1 \mathcal{L}_{vssim} + \gamma_2 \mathcal{L}_{grad} \tag{2}$$

Here, $\mathcal{L}_{ssim}$ measures the global structural similarity between the warped prediction I_p and target I_t:

$$\mathcal{L}_{ssim} = 1 - SSIM(I_p, I_t) \tag{3}$$

To prevent vessel degradation, $\mathcal{L}_{vssim}$ applies a vascular-aware weighted SSIM. Using multi-scale Hessian responses V_p and V_t, we generate a spatial weight map W to penalize tubular region errors:

$$W = 1 + \alpha \frac{|V_p - V_t|}{\mu(|V_p - V_t|) + \epsilon} \tag{4}$$

$$\mathcal{L}_{vssim} = 1 - SSIM(W \odot I_p, W \odot I_t) \tag{5}$$

where $\mu(\cdot)$ denotes the global mean, ϵ ensures numerical stability, and $\odot$ is the Hadamard product.

Finally, $\mathcal{L}_{grad}$ enforces spatial gradient consistency via Sobel operators (∇_x, ∇_y) [4]to sharpen vessel boundaries and suppress blurring:

$$\mathcal{L}_{grad} = \|\nabla_x I_p - \nabla_x I_t\|_2^2 + \|\nabla_y I_p - \nabla_y I_t\|_2^2 \tag{6}$$

3 Experiment

3.1 Datasets and Evaluation Metrics

The datasets used in our experiments consist of two main parts: the public UDIS-D dataset[20] and a custom-built CLE liver microvasculature dataset (CLE-LMV). UDIS-D contains 10,440 pairs of 512×512 resolution training samples from natural scenes, exhibiting rich parallax and complex geometric variations.

To address the fine-tuning and evaluation needs in medical scenarios, we constructed the CLE-LMV dataset using a custom near-infrared (NIR) CLE system (Fig. 1) to image *ex vivo* mouse hepatic microvasculature. Initially, 1,510 high-resolution (1024×1024) raw images were acquired, preprocessed via linear interpolation [11] to remove honeycomb artifacts and partitioned into mutually exclusive training and testing sets at an 8:2 ratio. Subsequently, to closely replicate the physical and optical artifacts inherent in real CLE scans, we applied continuous sliding cropping to mimic the dynamic motion of the endomicroscopic probe. Furthermore, we introduced perspective distortion [19] to simulate non-rigid tissue deformations caused by probe pressure, and employed path-anchored illumination to emulate uneven light distribution. The final dataset comprises 10,000 sets of five consecutive overlapping images at a resolution of 128×128, with overlap rates ranging from 10% to 50%, including 8000 sets for training and 2000 sets for testing.

To rigorously assess the stitching quality, we employ the masked evaluation metrics introduced by Nie *et al.* [24]: masked Root Mean Square Error (mRMSE), masked Peak Signal-to-Noise Ratio (mPSNR), and masked Structural Similarity (mSSIM). In addition, we also calculated the Success Rate(%), which is the proportion of successfully stitched groups [18].

3.2 Implementation Details

We first pre-train model using the UDIS-D dataset for 100 epochs. Then we use the proposed CLE-LMV for fine-tuning with 50 epochs.The model is optimized using Adam [13], starting with an initial learning rate of 10^{-4} and decaying to 10^{-5} for fine-tuning.The hyperparameters for the loss function are empirically set as $\lambda_1 = \lambda_2 = \lambda_3 = 1$, $\lambda_4 = 0.5$, $\lambda_4 = 0.5$, $\gamma_1 = 2$, $\gamma_2 = 0.5$. All implementations are based on PyTorch using two NVIDIA Tesla A100 GPUs.

3.3 Quantitative Comparison

We compared our method with 4 traditional stitching algorithms: SIFT, APAP, SPW, LPC and 4 learning-based methods: UDIS2, StabStitch2, RopStitch, SV-UDIS. The results are shown in Table 1, where $I_{3\times3}$ is the identity matrix,

representing the unaligned target image as a reference. The baseline methods were implemented by their best model according to official codes.

Traditional methods like APAP achieve favorable mRMSE and mPSNR but suffer from an unacceptably low Success Rate (6.25%), indicating severe feature matching failures on complex microscopic sequences. Conversely, deep learning baselines such as StabStitch2 guarantee a 100% Success Rate but severely compromise alignment accuracy (e.g., mSSIM of 0.5870), struggling to model non-rigid soft tissue deformations. In contrast, our fine-tuned Angio-Stitch achieves the optimal balance between extreme robustness and high-fidelity alignment. It delivers a perfect 100% Success Rate alongside the highest structural similarity (mSSIM of 0.9230) and highly competitive mRMSE (9.8122) and mPSNR (30.0817), comprehensively outperforming state-of-the-art methods for clinical multi-image stitching.

Table 1. Quantitative results on CLE-LMV. **Bold** and Underline indicate the best and second-best results, respectively.

Methods	mRMSE ↓	mPSNR ↑	mSSIM ↑	Success Rate(%)
$I_{3\times3}$	36.8566	17.2272	0.4682	-
SIFT[17]+RANSAC[7]	14.6297	25.5142	0.7907	5.85
APAP[30]	**6.5077**	**34.0142**	0.7885	6.25
LPC[12]	15.8924	26.1981	0.5780	10.40
SPW[16]	21.1905	25.2199	0.4225	5.25
UDIS2[22]	26.8324	20.4714	0.7126	25.40
StabStitch2[23]	23.7493	21.4335	0.5870	**100.00**
RopStitch[24]	21.0833	22.3671	0.6137	33.60
SV-UDIS[15]	25.6164	20.9121	0.8655	13.40
Ours	25.5492	20.9490	0.8679	48.45
Ours(fine-tuned)	9.8122	30.0817	**0.9230**	**100.00**

3.4 Qualitative Comparison

Fig. 3 shows the qualitative results of multi-image stitching on CLE-LMV. Other unshowned methods failed on this image set. The yellow rectangles and arrows indicates occurrences of deformation and distortion, while the red rectangles and arrows highlight the vascular stitching abnormal regions.

As observed, existing state-of-the-art methods suffer from severe cumulative errors on continuous sequences, resulting in global geometric distortions and structural collapse. In contrast, our method suppresses cumulative errors, accurately models soft tissue deformation, and preserves microvascular topological

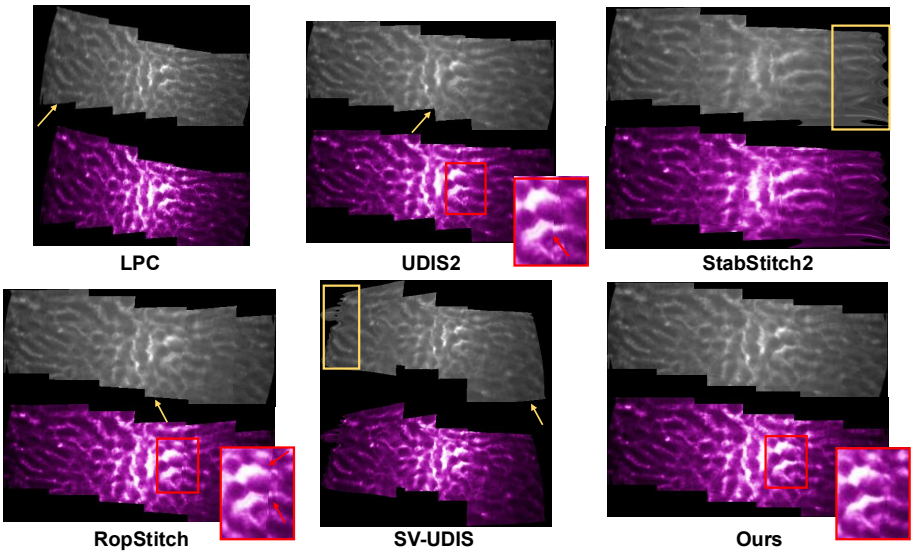

Fig. 3. Qualitative results on CLE-LMV. From left to right, top to bottom: the stitched results and Pseudo-color images.

continuity without ghosting, demonstrating its ability to provide high-fidelity wide-field panorama for reliable clinical diagnosis.

3.5 Ablation Studies

We conducted ablation studies on the CLE-LMV dataset to evaluate the two core components of Angio-Stitch (Table 2). Removing VPT leads to a notable decrease in mSSIM (-0.1144), highlighting its importance for robust feature matching under speckle noise. Similarly, excluding VSL increases mRMSE by +6.2015, highlighting the critical role of $\mathcal{L}_{vsl}$ in constraining non-rigid deformations and preserving microvascular topology. Overall, the complete model achieves the best performance, demonstrating the strong synergy between VPT and $\mathcal{L}_{vsl}$ to enable high-fidelity multi-image stitching.

4 Conclusion

In this paper, we propose Angio-Stitch, an unsupervised deep learning framework for multi-image stitching of CLE hepatic microvascular sequences. To overcome the inherently narrow FoV of CLE and the severe cumulative errors plaguing existing methods, our framework leverages a robust coarse-to-fine alignment strategy to accurately model complex non-rigid tissue deformations. Extensive quantitative and qualitative experiments on the CLE-LMV dataset demonstrate that Angio-Stitch achieves state-of-the-art performance. Future work will focus on extending this framework to broader optical biopsy modalities.

Table 2. Ablation studies on CLE-LMV. **Bolded** values indicate the best performance.

Configurations	mRMSE ↓	mPSNR ↑	mSSIM ↑
w/o VPT	29.0232	19.7845	0.7535
w/o VSL	31.7507	18.7701	0.8622
ours	**25.5492**	**20.9490**	**0.8679**

Acknowledgments. This research was supported by the Cross-disciplinary Collaboration Original Project Cultivation Funding Program of Department of General Surgery Sir Run-Run Shaw Hospital School of Medicine, and Department of Biomedical Engineering, Zhejiang University (Grant Nos. 114105-I22402), the Key Research and Development Plan of Zhejiang Province (Grant No. 2023C03094, 2024C03008).

Disclosure of Interests. The authors have no competing interests to declare that are relevant to the content of this article.

References

1. Abdel-Aziz, Y., Karara, H., Hauck, M.: Direct linear transformation from comparator coordinates into object space coordinates in close-range photogrammetry*. Photogrammetric Engineering & Remote Sensing **81**(2), 103–107 (2015)
2. Bookstein, F.: Principal warps: thin-plate splines and the decomposition of deformations. IEEE Transactions on Pattern Analysis and Machine Intelligence **11**(6), 567–585 (1989)
3. Chen, J., Frey, E.C., He, Y., Segars, W.P., Li, Y., Du, Y.: Transmorph: Transformer for unsupervised medical image registration. Medical Image Analysis **82**, 102615 (2022)
4. Chien, Y.: Pattern classification and scene analysis. IEEE Transactions on Automatic Control **19**(4), 462–463 (1974)
5. Chui, H., Rangarajan, A.: A new algorithm for non-rigid point matching. In: Proceedings IEEE Conference on Computer Vision and Pattern Recognition. CVPR 2000 (Cat. No.PR00662). vol. 2, pp. 44–51 vol.2 (2000)
6. DeTone, D., Malisiewicz, T., Rabinovich, A.: Deep image homography estimation. CoRR **1606.03798** (2016)
7. Fischler, M.A., Bolles, R.C.: Random sample consensus: a paradigm for model fitting with applications to image analysis and automated cartography. Commun. ACM **24**(6), 381–395 (Jun 1981)
8. Gong, L., Wang, H., Zuo, S.: Intensity-based nonrigid endomicroscopic image mosaicking incorporating texture relevance for compensation of tissue deformation. Computers in Biology and Medicine **142**, 105169 (2022)
9. Han, W., Kong, R., Wang, N., Bao, W., Mao, X., Lu, J.: Confocal laser endomicroscopy for detection of early upper gastrointestinal cancer. Cancers **15**(3), 776 (Jan 2023)
10. He, K., Zhang, X., Ren, S., Sun, J.: Deep residual learning for image recognition. In: 2016 IEEE Conference on Computer Vision and Pattern Recognition (CVPR). pp. 770–778 (2016)

11. Hughes, M.R.: Real-timing processing of fiber bundle endomicroscopy images in Python using PyFibreBundle. Applied Optics **62**(34), 9041 (dec 2023)
12. Jia, Q., Li, Z., Fan, X., Zhao, H., Teng, S., Ye, X., Latecki, L.J.: Leveraging line-point consistence to preserve structures for wide parallax image stitching. In: 2021 IEEE/CVF Conference on Computer Vision and Pattern Recognition (CVPR). pp. 12181–12190 (2021)
13. Kingma, D.P., Ba, J.: Adam: A method for stochastic optimization. CoRR **1412.6980** (2014)
14. Li, L., Mazomenos, E., Chandler, J.H., Obstein, K.L., Valdastri, P., Stoyanov, D., Vasconcelos, F.: Robust endoscopic image mosaicking via fusion of multimodal estimation. Medical Image Analysis **84**, 102709 (2023)
15. Liang, H., Dong, Z., Chen, K., Li, H., Guo, J., Yue, Y., Fu, M., Yang, Y.: Chatstitch: Visualizing through structures via surround-view unsupervised deep image stitching with collaborative llm-agents. IEEE Transactions on Circuits and Systems for Video Technology pp. 1–1 (2025)
16. Liao, T., Li, N.: Single-perspective warps in natural image stitching. IEEE Transactions on Image Processing **29**, 724–735 (2020)
17. Lowe, D.G.: Distinctive image features from scale-invariant keypoints. Int. J. Comput. Vision **60**(2), 91–110 (nov 2004)
18. Mei, Y., Yang, L., Wang, M., Yu, T., Wu, K.: Dunhuangstitch: Unsupervised deep image stitching of dunhuang murals. IEEE Transactions on Visualization and Computer Graphics **31**(8), 4226–4240 (2025)
19. Nie, L., Lin, C., Liao, K., Liu, M., Zhao, Y.: A view-free image stitching network based on global homography. Journal of Visual Communication and Image Representation **73**, 102950 (2020)
20. Nie, L., Lin, C., Liao, K., Liu, S., Zhao, Y.: Unsupervised deep image stitching: Reconstructing stitched features to images. IEEE Transactions on Image Processing **30**, 6184–6197 (2021)
21. Nie, L., Lin, C., Liao, K., Liu, S., Zhao, Y.: Depth-aware multi-grid deep homography estimation with contextual correlation. IEEE Transactions on Circuits and Systems for Video Technology **32**(7), 4460–4472 (2022)
22. Nie, L., Lin, C., Liao, K., Liu, S., Zhao, Y.: Parallax-tolerant unsupervised deep image stitching. In: 2023 IEEE/CVF International Conference on Computer Vision (ICCV). pp. 7365–7374 (2023)
23. Nie, L., Lin, C., Liao, K., Zhang, Y., Liu, S., Zhao, Y.: Stabstitch++: Unsupervised online video stitching with spatiotemporal bidirectional warps. IEEE Transactions on Pattern Analysis and Machine Intelligence **47**(9), 7443–7456 (2025)
24. Nie, L., Mei, Y., Liao, K., Xu, X., Lin, C., Xiao, B.: Robust image stitching with optimal plane. IEEE Transactions on Visualization and Computer Graphics pp. 1–11 (2026)
25. Perperidis, A., Dhaliwal, K., McLaughlin, S., Vercauteren, T.: Image computing for fibre-bundle endomicroscopy: A review. Medical Image Analysis **62**, 101620 (2020)
26. Pilonis, N.D., Januszewicz, W., di Pietro, M.: Confocal laser endomicroscopy in gastro-intestinal endoscopy: technical aspects and clinical applications. Translational Gastroenterology and Hepatology **7**(0) (2020)
27. Schneider, C., Johnson, S.P., Gurusamy, K.S., Cook, R.J., Desjardins, A.E., Hawkes, D.J., Davidson, B.R., Walker-Samuel, S.: Identification of liver metastases with probe-based confocal laser endomicroscopy at two excitation wavelengths. Lasers in Surgery and Medicine **49**, 280 – 292 (2016)

28. Tang, Y., Anandasabapathy, S., Richards-Kortum, R.: Advances in optical gastrointestinal endoscopy: a technical review. Molecular Oncology **15**(10), 2580–2599 (2020)
29. Vercauteren, T., Perchant, A., Malandain, G., Pennec, X., Ayache, N.: Robust mosaicing with correction of motion distortions and tissue deformations for in vivo fibered microscopy. Medical Image Analysis **10**(5), 673–692 (2006)
30. Zaragoza, J., Chin, T.J., Brown, M.S., Suter, D.: As-projective-as-possible image stitching with moving dlt. In: 2013 IEEE Conference on Computer Vision and Pattern Recognition. pp. 2339–2346 (2013)